# A Large-Stroke Flexure Fast Tool Servo with New Displacement Amplifier

Hao Liang[1], Hui Tang[1], Lixiong Huang[1], Jian Gao[1], Xin Chen[1], Suet To[2], Yangmin Li[2], *Senior Member*, IEEE, Yunbo He[1]

***Abstract*—As the rapid progress of science and technology, the free-form surface optical component has played an important role in spaceflight, aviation, national defense, and other areas of the technology. While the technology of fast tool servo (FTS) is the most promising method for the machining of free-form surface optical component. However, the shortcomings of short-stroke of fast tool servo device have constrained the development of free-form surface optical component. To address this problem, a new large-stroke flexible FTS device is proposed in this paper. A series of mechanism modeling and optimal designs are carried out via compliance matrix theory, pseudo-rigid body theory, and Particle Swarm Optimization (PSO) algorithm, respectively. The mechanism performance of the large-stroke FTS device is verified by the Finite Element Analysis (FEA) method. For this study, a piezoelectric (PZT) actuator P-840.60 that can travel to 90 μm under open-loop control is employed, the results of experiment indicate that the maximum of output displacement can achieve 258.3μm, and the bandwidth can achieve around 316.84 Hz. Both theoretical analysis and the test results of prototype uniformly verify that the presented FTS device can meet the demand of the actual microstructure processing.**

***Keywords*—Fast tool servo, lever displacement amplifier, flexure, large-stroke, microstructure**

## I. INTRODUCTION

As a special kind of curved surface, the complex micro structured surface has been widely used in various fields because of its remarkable advantages such as improving the optical performance, optimizing the product structure and realizing the lightweight. However, such curved surface has a rather complex structure with no fixed rotary center shaft, which requires the accuracy of the sub-micron surface shape and the roughness of the nanoscale surface. Therefore, the nanofabrication of complex microstructure optical component has become a big worldwide problem. The traditional processing technology of manufacturing is difficult to meet the processing needs of complex microstructure optical element because of its low accuracy and low efficiency. And the technology of fast tool servo (FTS) is regarded as the most promising nanofabrication method of the free-form surface optical component due to its high speed, high precision and high efficiency [1-3].

A few of institutions have focused on the research on FTS since Lawrence national laboratory in the United States developed a FTS for the first time [4]. As we know, flexure-based compliant mechanism has no friction and small transmission clearance without assembly, abrasion and lubrication, which can realize ultra-high precision movement and store elastic energy. In addition, compared with other actuator, piezoelectric actuator is featured with large driving force and nanometer resolution, thus most of the commercialized FTS devices use it to drive the flexure-guided structure. Unfortunately, the traditional PZT-actuated FTS device can only realize high frequency reciprocating motion with small travel range, which leads to difficulties in the nanofabrication of the complex free-form surface optical component, as well as restricts the development of the complex microstructure optical component. A few of research teams have focused on the technology of long stroke FTS. However, these devices often can't fulfill the task in the case of high speed and high precision [5]. To meet this requirement, a large-stroke flexure fast tool servo with a new displacement amplifier is presented in this paper.

The common flexible displacement amplifier includes: (1) amplification mechanism based on the lever principle;(2) bridge-type displacement amplification mechanism;(3) Scott-Russell amplification mechanism, etc.. Among these amplifiers, lever displacement amplifier is the most extensively used in the compliant mechanisms since it has simple structure, good rigidity, and can keep a linear function between the input and output displacement [6]. Hence, a novel lever displacement amplifier has been designed and applied to drive the FTS device. A series of mechanism modeling and optimal designs are carried out via compliance matrix theory, pseudo-rigid body theory, and PSO algorithm, respectively. Finally, the mechanism performance of the large-stroke FTS device is verified through the ANSYS Workbench platform.

What we have done is the design and analysis of a novel large-stroke FTS device with a new designed lever

*This work was supported in part by Natural Science Foundation of China (5160051494),Guangdong General Programs for Science and Technology Development(2015A010104009),Science and Technology Program of Guangzhou(201510010058),Natural Science Foundation of Guangdong Province(2014A030310204),Natural Science Foundation of China (51675106,51575544),Guangdong application-oriented R&D projects (2015B010133005).

H. Liang, H. Tang, L. Huang, J. Gao, X. Chen, and Y. He are with Department of Electromechanical Engineering, Guangdong University of Technology, Higher Education Mega Center, Guangzhou, China.

S. To and Y. Li are with Department of Industrial and Systems Engineering,The Hong Kong Polytechnic University, Hung Hom, Kowloon, Hong Kong SAR, China. Corresponding authors: huitang@gdut.edu.cn(Hui Tang); yangmin.li@polyu.edu.hk (Yangmin Li).

displacement amplifier. The framework of this paper is described as follows: the mechanism design of FTS is presented in Section II; the mechanism modeling and dimension optimization are worked out in Section III; the FEA analysis and evaluation are implemented in Section IV; ultimately, the achievements are summed up with future work indicated in Section V.

## II. Design of FTS Device

### A. Design of the Whole Structure

The objective of this work is to design a new 1-DOF fast tool servo mechanism with long-stroke. As shown in Fig.1, right-circular flexure hinge and corner-filleted flexure hinge are adopted in this design. The right-circular flexure hinge is of higher movement precision, but its rotational range is relatively smaller; the straight-beam flexible hinge is of larger rotation range, but its movement precision is poorer. And the corner-filleted flexible hinge movement takes into account both motion precision and travel range. Therefore, in the design of the flexible displacement amplifier of the FTS device, the right-circular flexure hinge is chosen where high accuracy should be considered, and the corner-filleted flexible hinge is chosen where the movement precision and range of motion should be considered at the same time. In addition, in a drive to increase the dynamic performance of FTS system, a material with high elastic modulus $E$ and low density $\rho$ is required on account that the rigid and light-weight materials (high $E$ and low $\rho$) can improve the stiffness and bandwidth of FTS [7]. In this study, Aluminum alloy 7075 with a relatively high value of $E/\rho$ (see Table I) is chosen to fabricate the FTS device.

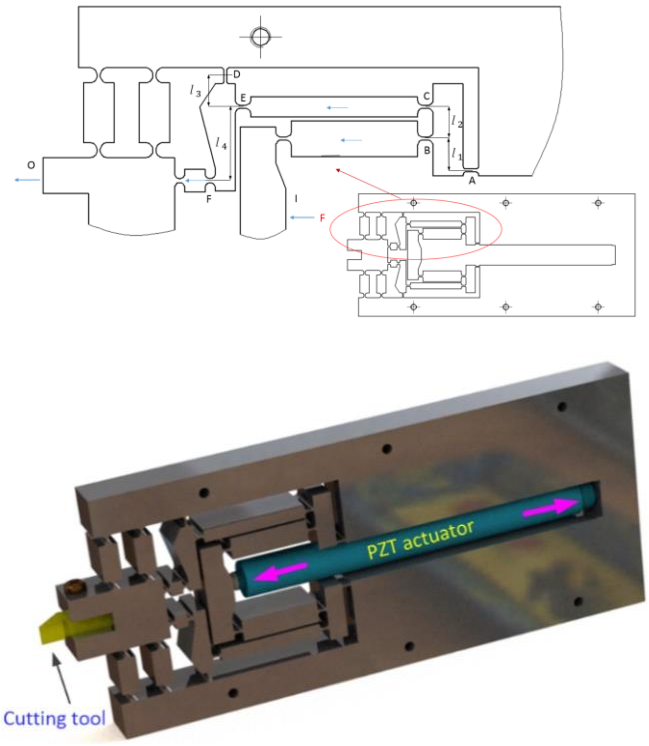


Fig. 1. The designed FTS mechanism.

Table I
THE PARAMETERS OF AL7075-T6 MATERIAL

| Material parameters | | | |
|---|---|---|---|
| E | σ | ν | ρ |
| 71.7 GPa | 503 MPa | 0.33 | $2.81 \times 10^3 Kg/m^3$ |

### B. Design of Flexible Displacement Amplifier

In order to ensure the vertical stiffness and horizontal stiffness of the FTS device, the output of the flexible displacement amplifier needs to be added with a compliant translational joint. The flexible moving mechanism formed by the flexible hinge mechanism mainly consists of a single parallel four-bar flexible hinge mechanism(See Fig.2) and a double parallel four-bar flexible hinge mechanism(See Fig.3). The former one will produce a cross coupling error in the vertical direction under the action of force [7].

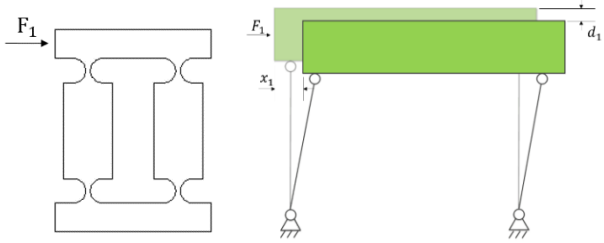


Fig. 2. Single parallel four-bar flexible hinge mechanism.

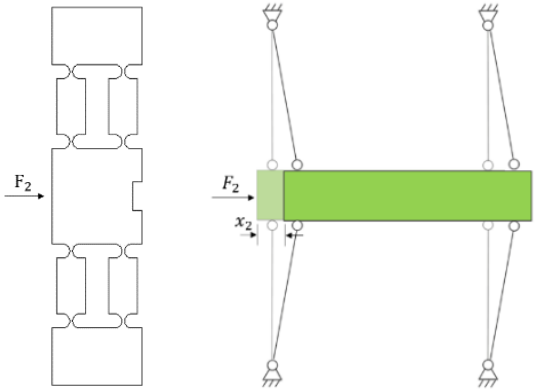


Fig. 3. Double parallel four-bar flexible hinge mechanism.

The schematic diagram of a lever displacement amplification mechanism is depicted in Fig.4. Once the PZT actuator output a displacement, the device produces a larger displacement. Generally, this type of displacement amplifier based on the lever principle possesses the following merits: 1) the simple structure and the small mechanism dimension; 2) the symmetrical structure, and it can output high precision motion, because of the high rigidity of this amplification mechanism. Hence, the lateral coupling displacement error of this mechanism can be completely eliminated theoretically. Therefore, it is quite suitable for constructing a FTS device.

According to practical requirements, two levers are employed to increase the stroke and achieve a compact structure [8]. In addition, the corner-filleted hinge is adopted

because of its high movement precision and large rotational range. The models for predicting of displacement amplification ratio are established in next sections.

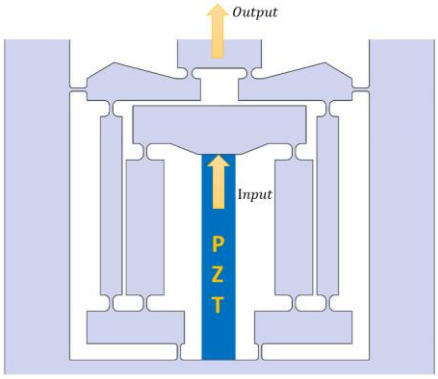


Fig. 4. The designed flexible displacement amplifier.

## III. Mechanism Modeling and Optimization

### A. Modeling of Amplifier Output Lever

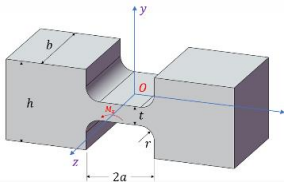

Fig. 5. Corner-filleted hinge

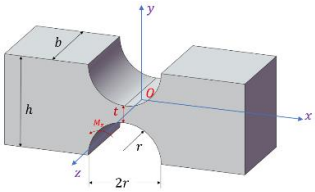

Fig. 6. Right circular hinge

For corner-filleted flexible hinge, $\beta = \frac{t}{2r}$ , $\gamma = \frac{t}{2a}$

For right circular flexible hinge, $\alpha = \frac{t}{2r}$ , $\psi = \frac{h}{2r}$

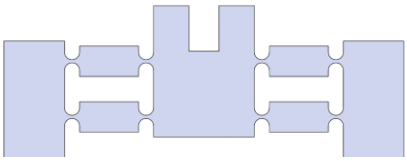

Fig. 7. Double parallel four-bar flexible hinge mechanism.

Then, the input stiffness of the double parallel four-bar flexible hinge mechanism (see Fig.7) can be derived as follows,

$$K_t = \frac{F_o}{L_o} = \frac{3l^2}{2Ebr^2(2\alpha+\alpha^2)}\left\{\left[\frac{1+\alpha}{\psi^2}+\frac{3+2\alpha+\alpha^2}{\psi(2\alpha+\alpha^2)}\right]\sqrt{1-(1+\alpha-\psi)^2}+\frac{6(1+\alpha)}{(2\alpha+\alpha^2)^{3/2}}\tan^{-1}\left[\frac{\psi-\alpha}{\sqrt{1-(1+\alpha-\psi)^2}}\sqrt{\frac{2+\alpha}{\alpha}}\right]\right\} \quad (3\text{-}1)$$

where $l$ is the lever length of the double parallel four-bar flexible hinge mechanism, $E$ is the elastic modulus of the material, $F_o$ is the output force of the lever and $L_o$ is the output displacement of the lever.

Also, the rotational stiffness of the corner-filleted flexible hinge can be derived as follows,

$$K = \frac{Ebt^3r^2}{12lr^2+12ft^3} \quad (3\text{-}2)$$

where $r$ is the fillet radius; $E$ is the elastic modulus of the material,

$$f = \int_{-\frac{\pi}{2}}^{\frac{\pi}{2}} \frac{\cos\theta}{\left(\frac{t}{r}+2-2\cos\theta\right)^3}d\theta$$

Afterwards, the displacement relationship of flexure hinge can be expressed as follows,

$$\begin{bmatrix}\theta\\ \Delta y\\ \Delta x\end{bmatrix} = \begin{bmatrix}C_{\theta,M_z} & C_{\theta,F_y} & 0\\ C_{y,M_z} & C_{y,F_y} & 0\\ 0 & 0 & C_{x,F_x}\end{bmatrix}\begin{bmatrix}M_z\\ F_y\\ F_x\end{bmatrix} \quad (3\text{-}3)$$

where $C_{\theta,M_z} = \frac{12}{Eb}(f_1' + f_1'')$

$$C_{\theta,F_y} = C_{y,M_z} = \frac{12}{Eb}(af_1' + af_1'' - f_2' - f_2'')$$

$$C_{y,F_y} = \frac{12}{Eb}(a^2f_1' + a^2f_1'' - 2af_2' - 2af_2'' + f_3' + f_3'')$$

$$C_{x,F_x} = \frac{1}{Eb}(f_4' + f_4'')$$

For corner-filleted flexible hinge,

$$f_1' = f_1'' = \frac{1}{4t^2}\left[\frac{2}{\gamma}-\frac{2}{\beta}+\frac{2\beta^2+4\beta+3}{(\beta+1)(\beta+2)^2}+\frac{6(\beta+1)}{\sqrt{\beta}(\beta+2)^{2.5}}tan^{-1}\sqrt{\frac{2}{\beta}+1}\right]$$

$$f_2' = f_2'' = -\frac{1}{8t\beta}\left\{\frac{\beta-\gamma}{(\beta+2)^2\gamma}\left[\frac{2\beta^2+4\beta+3}{(\beta+1)(\beta+2)^2}+\frac{6(\beta+1)}{\sqrt{\beta(\beta+2)}}\tan^{-1}\sqrt{\frac{2}{\beta}+1}\right]+\frac{1}{\beta+1}\right\}-\frac{(\beta-\gamma)^2}{8t\beta^2\gamma^2}$$

$$f_3' = f_3'' = -\frac{1}{16\gamma^2}\left[\frac{2}{\gamma}-\frac{2}{\beta}+\frac{2\beta^2+4\beta+3}{(\beta+1)(\beta+2)^2}+\frac{6(\beta+1)}{\sqrt{\beta}(\beta+2)^{2.5}}tan^{-1}\sqrt{\frac{2}{\beta}+1}\right]+\frac{1}{8}\left\{\frac{(\beta-\gamma)(4\beta^2-2\beta\gamma+\gamma^2)}{3\beta^3\gamma^3}+\frac{2\beta^2+4\beta+3}{(\beta+1)(\beta+2)^2\gamma^2}+\frac{2\beta^3+6\beta^2+3\beta-5+2\beta(1-\beta)/\gamma}{2[\beta(\beta+2)]^2}+\frac{(\beta+1)(3+2\beta-7\beta^2-8\beta^3-2\beta^4+6\beta^2/\gamma^2-6\beta/\gamma)}{[\beta(\beta+2)]^{2.5}}\tan^{-1}\sqrt{\frac{2}{\beta}+1}+\frac{\pi}{2}\right\}$$

$$f_4' = f_4'' = \frac{\beta-\gamma}{2\beta\gamma}+\frac{\beta+1}{\sqrt{\beta(\beta+2)}}\tan^{-1}\sqrt{\frac{2}{\beta}+1}-\frac{\pi}{4}$$

The parameters without superscript denotes the analyzed lever, while the parameters with superscript " ' " denotes the first lever and the parameters with superscript " " " denotes the second one.

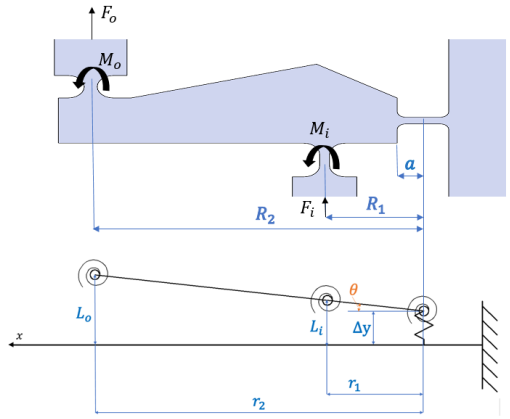


Fig. 8. The output lever model of flexible displacement amplifier.

From (3-2), we gain $\Delta y = F_iY_1 + F_oY_2 + M_zC_{y,M_z}$ (3-4)

$$\theta = F_iY_3 + F_oY_4 + M_zC_{\theta,M_z} \quad (3\text{-}5)$$

where $M_z = M_i + M_o$, $Y_1 = C_{y,F_y} + r_1C_{y,M_z}$, $Y_2 = C_{y,F_y} + r_2C_{y,M_z}$

$Y_3 = C_{\theta,F_y} + r_1C_{\theta,M_z}$, $Y_4 = C_{\theta,F_y} + r_2C_{\theta,M_z}$, $r_1 = R_1 - a$, $r_2 = R_2 - a$

From geometrical relationship (see Fig.8), we get

$$\theta = \frac{L_i - \Delta y}{r_1} \tag{3-6}$$

$$L_o = \Delta y + r_2\theta \tag{3-7}$$

$$M_i = -K(\theta + \frac{L_i}{r_2'}) \tag{3-8}$$

$$M_o = -K(\theta + \frac{L_o}{r_1''}) \tag{3-9}$$

From (3-4) to (3-9), we get

$$\Delta y = \frac{Y_5+Y_6}{Y_5+Y_7}L_i + \frac{Y_2Y_3-Y_1Y_4}{Y_3(Y_5+Y_7)}F_o \tag{3-10}$$

$$\theta = \frac{Y_7-Y_6}{r_1(Y_7+Y_5)}L_i - \frac{Y_2Y_3-Y_1Y_4}{r_1Y_3(Y_5+Y_7)}F_o \tag{3-11}$$

$$L_o = Y_8L_i + Y_9F_o \tag{3-12}$$

$$F_i = Y_{10}L_i - Y_{11}F_o \tag{3-13}$$

where $Y_5 = \frac{Y_1+(p_i+p_o)(Y_1-C_{y,M_z}KY_3)}{r_1Y_3}$

$$Y_6 = -\frac{C_{y,M_z}KY_3-Y_1}{Y_3}\left(\frac{1}{q_ir_2'}+\frac{m}{q_or_1''}\right)$$

$$Y_7 = 1+\frac{C_{y,M_z}KY_3-Y_1}{q_or_1''Y_3}(1-m)$$

$$Y_8 = \frac{Y_5+Y_6+m(Y_7-Y_6)}{Y_5+Y_7}$$

$$Y_9 = \frac{(1-m)(Y_2Y_3-Y_1Y_4)}{Y_3(Y_5+Y_7)}$$

$$Y_{10} = \frac{(1+p_i+p_o)(Y_7-Y_6)}{r_1Y_3(Y_5+Y_7)}+\frac{1}{Y_3}\left(\frac{1}{q_ir_2'}+\frac{Y_8}{q_or_1''}\right)$$

$$Y_{11} = \frac{(1+p_i+p_o)(Y_2Y_3-Y_1Y_4)}{r_1Y_3^2(Y_5+Y_7)}+\frac{Y_4}{Y_3}-\frac{Y_9}{q_or_1''Y_3}$$

$$\mathrm{m} = \frac{r_2}{r_1}$$

When the lever relative to the flexure hinge rotating, $p_i$ and $p_o$ are equal to 1. When the lever relative to the flexure hinge rotating in the opposite direction, $q_i$ and $q_o$ are equal to 1.

From (3-12), the amplification ratio of the output lever $A_2$ is derived as follows,

$$A_2 = \frac{L_o}{L_i} = \frac{Y_8}{1-Y_9K_t}$$

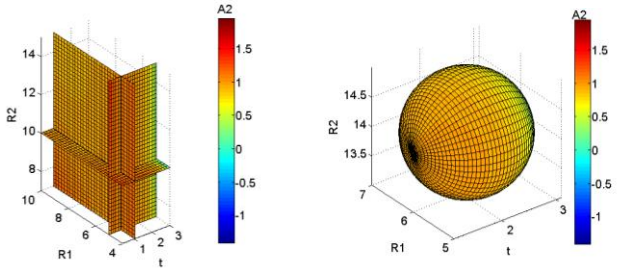


Fig. 9. The displacement amplification ratio with the variation of the dimension.

As shown in Fig.9, the color of figure indicates the magnitude of the amplification ratio and the coordinate value indicates the dimension of the output lever.

*B. Modeling of Amplification Ratio Based on Pseudo-Rigid Body Method*

*1) Modeling of amplification ratio based on the geometric relationship*

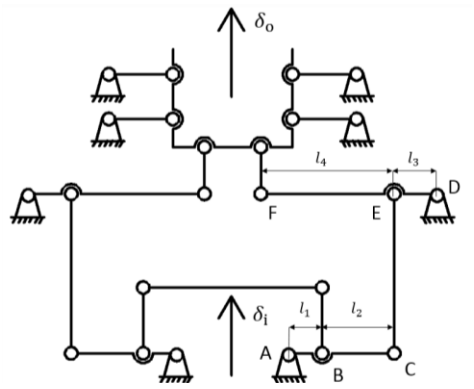


Fig 10. The schematic diagram of kinematics of the FTS.

To ensure that the FTS device is able to output a large displacement, a series of dimension optimizations have been conducted, which aims to improve the displacement amplification ratio of the flexible displacement amplifier. Its working principle is shown in Fig.10. On the basis of the principle of lever amplifier, the output displacement of the FTS device is derived as follows,

$$\delta_o = \frac{(l_1+l_2)(l_3+l_4)}{l_1l_3}\delta_i$$

where $\delta_i$ and $\delta_o$ are the input displacement and the output displacement, respectively. Thus, the displacement magnification ratio of the flexible displacement amplifier $A$ can be expressed as follows,

$$A = \frac{\delta_o}{\delta_i} = \frac{(l_1+l_2)(l_3+l_4)}{l_1l_3}$$

Also, the size optimization work is executed, which aims to increase the magnification ratio of the flexible displacement amplifier. However, due to the deformation of the flexible hinges, the established amplification ratio model based on the geometric relationship is different from the actual one. Therefore, in the following part, the deformations of the flexure hinges will be considered in our modeling work.

*2) Modeling of amplification ratio with consideration of flexure deformations*

Combining with (3-12) and (3-13), we get

$$L_o' = Y_8'L_i' + Y_9'F_o' \tag{3-14}$$

$$F_i' = Y_{10}'L_i' - Y_{11}'F_o' \tag{3-15}$$

$$L_o'' = Y_8''L_i'' + Y_9''F_o'' \tag{3-16}$$

$$F_i'' = Y_{10}''L_i'' - Y_{11}''F_o'' \tag{3-17}$$

Also, there exist the following relationships between the first lever and the second one,

$$F_i'' = -F_o' \tag{3-18}$$

$$L_i'' = L_o' \tag{3-19}$$

From (3-14) to (3-19), we get

$$A = \frac{L_o''}{L_i'} = \left(Y_8 - \frac{Y_8Y_{11}Y_{10}''}{1+Y_9Y_{10}''}+\frac{Y_9Y_{11}''}{1+Y_9Y_{10}''}\frac{F_o''}{L_i'}\right)\left(Y_8'' + \frac{Y_9''(1+Y_9Y_{10}'')}{Y_9Y_{11}''+Y_8L_i'/F_o''}\right)$$

As for the FTS device, the output force $F_o''$ will be measured in the actual situation, while $L_i'$ is equal to the input displacement of the PZT actuator, thus the displacement amplification ratio of the FTS device can be

obtained [8].

### C. Dimension Optimization with PSO

According to previous research, we can find out that the theoretical displacement amplification ratio of the flexible displacement amplifier based on the lever principle is always smaller than the actual one, the main reason of which is the deformation of the lever and the abnormal stretching or extrusion of the flexure hinges. Thus, the size of the flexible displacement amplifier of the FTS will be optimized via MATLAB PSOT toolbox. Details of the optimization are as follows,

1) Objection: Maximum value of displacement amplification ratio $A$;
2) Relevant parameters: $h, b, t, r, l_1, l_2, l_3, l_4$;
3) Ranges: $4.00\text{mm} \leqslant h \leqslant 10.00\text{mm}$, $0.30\text{mm} \leqslant R \leqslant 1.20\text{mm}$, $6.25\text{mm} \leqslant l_1 \leqslant 12.00\text{mm}$, $4.00\text{mm} \leqslant l_2 \leqslant 6.25\text{mm}$, $0.60\text{mm} \leqslant t \leqslant 1.00\text{mm}$, $6.10\text{mm} \leqslant l_3 \leqslant 10.00\text{mm}$, $6.25\text{mm} \leq l_4 \leq 14.60\text{mm}$.

Parameter $b$ is the thickness of the FTS device (15mm). Furthermore, in consideration of that the FTS device is fabricated by wire electro-discharge machining, the thickness of the flexible hinge $t$ is no less than 0.6mm. And parameter $l_1 \sim l_4$ is the lever arm length of the flexible displacement amplifier. As shown in Fig.11, the amplification ratio of the flexible displacement amplifier can reach to 3.33. The structural dimensions of the FTS device are shown in Table II.

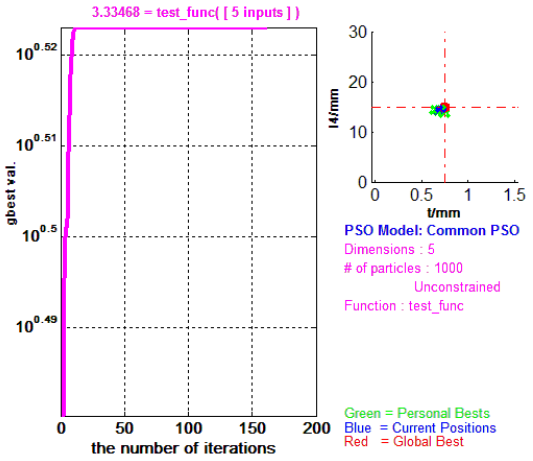


Fig.11. PSO dimension optimization results.

TABLE II
THE DIMENSION PARAMETERS OF THE OPTIMIZED FTS DEVICE
(mm)

| $h$ | $b$ | $t$ | $R$ | $l_1$ | $l_2$ | $l_3$ | $l_4$ |
|---|---|---|---|---|---|---|---|
| 6 | 15 | 0.6 | 0.5 | 6.25 | 6.25 | 6.10 | 14.6 |

## IV. FEA Analysis and Evaluation

As shown in Fig.12(a), the 3D finite element mesh of FTS is constructed by the ANSYS Workbench, and then the model in terms of the maximum output displacement analysis, strength checking, displacement amplification ratio calculation and modal analysis are conducted in details.

For the purpose of testing the maximum output displacement of the FTS device, a series of forces 0~1000N are applied to the input of the FTS device. As shown in Fig.12(b), when the input loads 1000N, the output displacement of the FTS device can reach to 123.47μm. It can be demonstrated that the flexible displacement amplifier can effectively increase the stroke of the FTS device even though the maximum output displacement of the piezoelectric actuator P-840.6 is 90μm.

With the purpose of checking the strength of the FTS device, the input force is 0 to 1000N at the input of the FTS device. As the Fig.12(c) shows, the maximum equivalent stress is 260.65MPa while the yield strength of Aluminum Alloy7075 is 503MPa, which indicates that the FTS device can withstand more than 1500N of the input load and meet the strength requirements.

To calculate the displacement magnification ratio of the flexible displacement amplification mechanism in the FTS device, when the input displacement of the FTS device is 40μm, as shown in Fig.12(d) and Fig.13, the output displacement is 114.9μm, and the displacement amplification ratio $A$ can be expressed as follows,

$$A = \frac{\delta_o}{\delta_i} = \frac{114.9\mu m}{40\mu m} = 2.8725$$

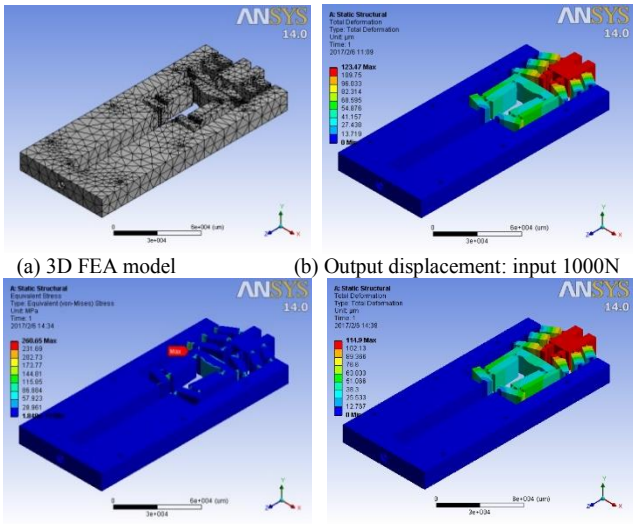


(a) 3D FEA model (b) Output displacement: input 1000N

(c) Stress analysis (d) Output displacement: input 40μm

Fig.12. The structural static analysis results.

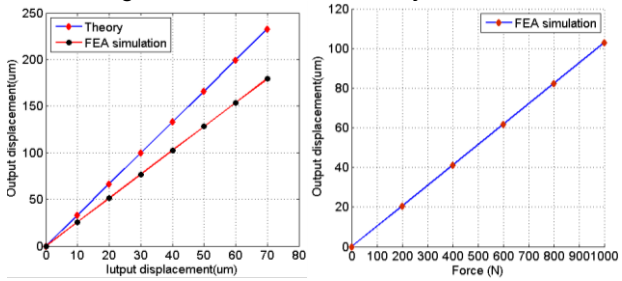


(a) (b)

Fig. 13. FEA and theory evaluation results.

Furthermore, to verify the dynamic performance of the FTS device, the modal analysis of the FTS device was carried out. As the Fig.14 (a-f) shows, the red region and the

blue region represent large deformation areas and small deformation areas, respectively. The resonance frequency of the first order denotes the natural work frequency of the FTS device is 316.84Hz, the other modal resonances occur in the mode 2~6 (much higher than 316.84Hz), which verifies that the FTS device can work in a high-rate manner without resonance.

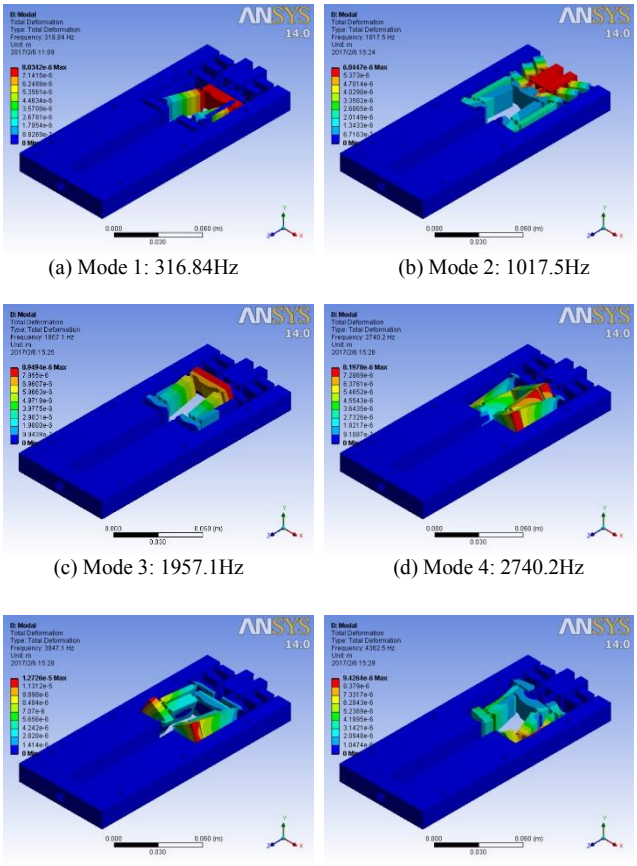

(a) Mode 1: 316.84Hz (b) Mode 2: 1017.5Hz

(c) Mode 3: 1957.1Hz (d) Mode 4: 2740.2Hz

(e) Mode 5: 3947.1Hz (f) Mode 6: 4362.5Hz

Fig. 14. The modal analysis results.

All of the simulation results uniformly verify that the presented FTS device has excellent performance that it can fulfill the work of high speed and high precision cutting.

## V. CONCLUSIONS

To cater for the requirements of large-travel nanofabrication of the free-form surface optical component, a new long-stroke fast tool servo device is presented in this paper. The achievements are listed as follows: 1) design of a 1-DOF FTS device with new flexible displacement amplifier; 2) modeling of the lever displacement amplifier, evaluating displacement amplification ratio, and optimizing its performance via compliance matrix theory, pseudo-rigid body theory, and Particle Swarm Optimization algorithm, respectively; 3) the verification and evaluation of the FTS device were carried out via ANSYS Workbench. Theoretical deduction and simulation results congruously confirm that the actual amplification ratio of the FTS device can reach to 2.8725; in the case of the input stroke of 90μm, the stroke of the FTS can reach to 258.3μm and its work frequency can achieve 316.84Hz. All the results powerfully verify that the presented FTS device has excellent performance for practical microstructure processing.

Even so, we will consider the fabrication of the experimental prototype, and further verify the performance of this FTS device through a series of micro/nano machining experiments.

## REFERENCES


[1] Z. Zhu, S. To, K. F. Ehmann, and X. Zhou, "Design, analysis, and realization of a novel piezoelectrically actuated rotary spatial vibration system for micro/nano-machining," *IEEE-ASME Trans. Mechatron.*, DOI 10.1109/TMECH.2017.2682983, In press.

[2] H. Lu, D. Lee, et al., "Modeling and machining evaluation of micro-structure fabrication by fast tool servo based diamond machining," *Precision Engineering*, 38.1(2014): 212-216.

[3] H. Wang and S. Yang. "Design and control of a fast tool servo used in noncircular piston turning process," *Mechanical Systems & Signal Processing* 36.1(2013):87-94.

[4] F. Tian, Yin. Z, and S. Li. "A novel long range fast tool servo for diamond turning," *International Journal of Advanced Manufacturing Technology* (2016):1-8.

[5] X. Zhu, X. Xu, et al., "A novel flexure-based vertical nanopositioning stage with large travel range," *Review of Scientific Instruments* 86.10(2015):105112.

[6] H. Tang and Y. Li, "Development and active disturbance rejection control of a compliant micro/nano positioning piezo-stage with dual-mode," *IEEE Transactions on Industrial Electronics*, vol. 61, no. 3, pp. 1475-1492, March 2014.

[7] H. Tang and Y. Li, "A new flexure-based Yθ nanomanipulator with nanometer scale positioning resolution and millimeter range workspace," *IEEE-ASME Trans. Mechatron.*, vol. 20, no. 3, pp. 1320-1330, June 2015.

[8] G. Chen, Y. Ma, and J. Li, "A tensural displacement amplifier employing elliptic-arc flexure hinges," *Sensors and Actuators A: Physical* 247 (2016): 307-315.